The optimal Stokes-Brinkman coupling for two-dimensional transverse flows in dual-scale fibrous porous media using the effective Navier slip approach

Cite as: Phys. Fluids **31**, 073108 (2019); https://doi.org/10.1063/1.5098094
Submitted: 31 March 2019 . Accepted: 08 July 2019 . Published Online: 30 July 2019

Jin Gang Lu (陆金刚), **Nam Sub Woo** (우남섭) **and Wook Ryol Hwang** (황욱렬)

Physics of Fluids ARTICLE scitation.org/journal/phf

The optimal Stokes-Brinkman coupling for two-dimensional transverse flows in dual-scale fibrous porous media using the effective Navier slip approach

Cite as: Phys. Fluids 31, 073108 (2019); doi: 10.1063/1.5098094
Submitted: 31 March 2019 • Accepted: 8 July 2019 •
Published Online: 30 July 2019

Jin Gang Lu (陆金刚),[1] Nam Sub Woo (우남섭),[2] and Wook Ryol Hwang (황욱렬)[1,a)]

AFFILIATIONS

[1]School of Mechanical and Aerospace Engineering, Research Center for Aircraft Parts Technology (ReCAPT), Gyeongsang National University, Jinju 52828, South Korea
[2]Extreme Resources Plant R&D, Korea Institute of Geoscience and Mineral Resources, Pohang 37559, South Korea

[a)]Author to whom correspondence should be addressed: wrhwang@gnu.ac.kr

ABSTRACT

Optimal values of the effective viscosity and the stress jump coefficient in the Stokes-Brinkman model with continuous and jump stress conditions, respectively, have been accurately characterized and then applied to solve various two-dimensional transverse dual-scale flows in fibrous porous media. In this work, the effective viscosity and the stress jump coefficient are determined such that the interfacial slip velocity can be identified to that in the effective Navier-slip description and therefore it naturally facilitates the accurate prediction of the slip velocity and its gradient (stress) at the fluid/porous interface along with the velocity fields in both the porous media and the pure fluid domain. With these optimal values of the effective viscosity and the stress jump coefficient, the Stokes-Brinkman coupling can be employed to accurately describe the dual-scale porous flow at low computational cost, which may provide an effective computational framework in investigating particle deposition/filtration and void transports within composites.

I. INTRODUCTION

Viscous incompressible flows through and over the porous media can be encountered widely in nature and in industries: contaminant transport or flooding with the groundwater flow,[1,2] enhanced oil recovery,[3,4] enhanced dispersion performance,[5,6] and the flow of resins in-between the porous fiber tows or fiber bundles in liquid composite molding (LCM).[7–9] Among others, flows in-between fiber tows are of particular interest in the present work, considering voids transport through a porous channel[10,11] or particle deposition on fiber tows for advanced functional composites materials.[12] In LCM, the spacing between the fiber tows is on the scale of millimeters, whereas the spacing between the fibers within a fiber bundle is on the order of microns, creating a dual-scale porous medium. The fluid flow in-between the fiber tows (inter-tow flow) needs to be coupled to the flow inside the fiber tows (intra-tow flow),[12] which yields additional complexities along with the presence of the velocity slip around the tow interface and sophisticated stress conditions.

It is widely accepted that Darcy's law can be applied to describe the macroscopic flow within the porous media. In describing a flow around the porous media, however, the velocity at the interface of the fluid/porous media has been found to be several orders greater than the Darcy velocity, which implies the existence of a boundary layer adjacent to the interface, in which the fluid velocity decreases rapidly from the interfacial slip velocity to the Darcy velocity. However, Darcy's equation is not compatible with the presence of such a boundary layer in a porous medium due to the absence of the viscous stress. To account for the boundary layer flow within porous media in close proximity of the interface, Brinkman[13] extended the traditional form of Darcy's law by adding the viscous stress term along with a pseudo viscosity, the so-called effective viscosity, in

analogy to the viscosity behavior of a dense swarm of particles (particle suspensions). The additional viscous stress, called the Brinkman term, accounts for viscous dissipation within the boundary layer. Brinkman's extension of Darcy's law is preferred mathematically and physically to the original Darcy's law in examining boundary layer effects.[14,15]

In case of slow flows over small scale porous architectures in the LCM process, flows within the pure fluid domain can be described by the Stokes equation, while flow within the porous media including the boundary layer can be expressed by the Brinkman equation. The combination of the Stokes equation and the Brinkman equation, the so-called Stokes-Brinkman coupling (S-B coupling), has been widely employed in analyses and numerical simulations of dual-scale flows through and over the fibrous porous media.[12,16–18] Assuming that a fluid is Newtonian with negligible inertia, the Stokes equation in the pure fluid region can be expressed as

$$-\nabla p_f + \mu \nabla^2 \boldsymbol{u}_f = 0. \tag{1}$$

The subscript "f" denotes "fluid" and μ is the fluid viscosity. Flow in the porous media with viscous dissipation is described by the Brinkman equation

$$-\nabla p_p + \mu_e \nabla^2 \boldsymbol{u}_p - \frac{\mu}{K}\boldsymbol{u}_p = 0. \tag{2}$$

The subscript "p" denotes the "porous media," μ_e is the effective viscosity, and K is the permeability of the porous media. By introducing a scalar parameter λ, which takes the value of zero in the fluid domain and one in the porous media, flows in both regions can be described by a single equation, i.e., the Stokes-Brinkman coupling,

$$-\nabla p + \mu \nabla^2 \boldsymbol{u} + \lambda\left((\mu_e - \mu)\nabla^2 \boldsymbol{u} - \frac{\mu}{K}\boldsymbol{u}\right) = 0. \tag{3}$$

Since the incompressibility is valid everywhere, the continuity equation, i.e., $\nabla \cdot \boldsymbol{u} = 0$, completes the governing equation set.

In the Stokes-Brinkman coupling for flows in dual-scale porous media, a critical issue arises in selecting the effective viscosity (μ_e) in the viscous dissipation term of the Brinkman equation [Eq. (2)]. There seem to be some requirements for the optimal choice of the effective viscosity, and they are described in Fig. 1. The effective viscosity in the Stokes-Brinkman coupling must be a function of the porous architecture, and once determined, it needs to facilitate to represent the velocity profile not only in the fluid region (see "1" in Fig. 1) but also in the porous media including the boundary layer ("3" and "4"). Moreover, the slip velocity at the interface has to be correctly predicted ("2") along with the fluid stress (velocity gradient) there ("5"). In addition, a seepage flow within the porous media and a partial velocity slip at the interface need to be described simultaneously and correctly, if the upstream flow is not parallel to the interface of the porous media.

A common agreement has not been made in the literature on this critical issue how to choose the effective viscosity and it is still questionable although the effective viscosity is often assumed to be identical to the fluid viscosity for simplicity.[19–21] In the original work of Brinkman,[13] the effective viscosity was identified to the effective viscosity of particle suspensions considering that the flow in the porous media is analogous to the swarm of particles such that $\mu_e/\mu = 1 + 2.5\phi_s$ in a dilute regime with a low solid volume fraction ϕ_s. Later Breugem[17] and Kołodziej *et al.*[22] doubted this choice since particles move with the fluid in case of particle suspension, while the porous skeleton is fixed in the flow through the porous media. Koplik *et al.*[23] derived the relative effective viscosity theoretically from the effective energy dissipation rate around a sphere embedded in a collection of dilute spherical grains and proposed the relationship $\mu_e/\mu = 1 - 0.5\phi_s$. Kim and Russel[24] predicted the effective viscosity from the bulk stress using the volume averaging method and reported that the effective viscosity is greater than the pure fluid viscosity. Starov and Zhdanov[25] derived the effective viscosity of porous media composed of equally sized spherical particles, and the effective viscosity in their work was expressed as $\mu_e/\mu = 1/(1-\phi_s)^{5/2}$.

Another important issue in the Stokes-Brinkman coupling is the boundary condition at the interface, which is usually defined in terms of the slip velocity and the traction. The velocity continuity must be satisfied, whereas either stress continuity or stress jump can be employed in the modeling of the Stokes-Brinkman approach. Based on the nonlocal volume-averaging technique, the stress jump boundary condition at the fluid/porous interface was first proposed by Ochoa-Tapia and Whitaker (OT-W model)[26,27] such that

$$\boldsymbol{n} \cdot \left(\boldsymbol{\sigma}_p - \boldsymbol{\sigma}_f\right) = \frac{\mu}{\sqrt{K}}\boldsymbol{T} \cdot \boldsymbol{u}, \quad \boldsymbol{T} = \beta \boldsymbol{I}. \tag{4}$$

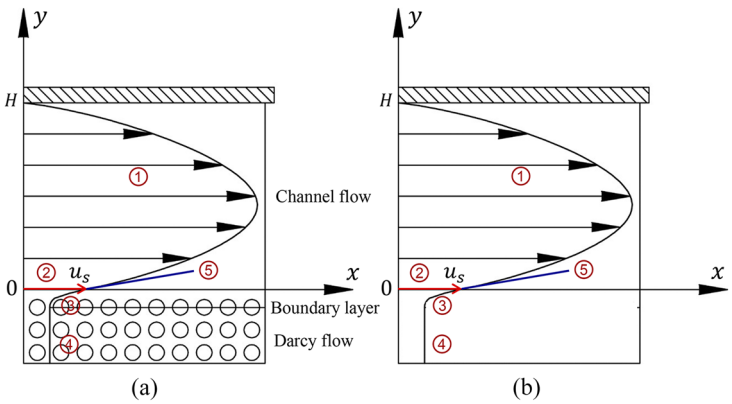

FIG. 1. The transverse flow over (a) a fibrous porous medium and over (b) a fictitious porous region with the effective slip in the view of the Stokes-Brinkman coupling.

The symbols $\boldsymbol{n}$, $\boldsymbol{\sigma}$, $\boldsymbol{T}$, $\boldsymbol{I}$, and β denote the outward normal vector at the interface, the total stress tensor, the stress jump tensor, the identity tensor, and the stress jump coefficient. As recommended in their works, the effective viscosity for the stress jump condition in the Brinkman equation is fixed as $\mu_e/\mu = 1/(1-\phi_s)$ and the stress jump coefficient tensor $\boldsymbol{T}$ is simplified as an isotropic tensor $\beta\boldsymbol{I}$, i.e., the stress discontinuity is assumed to be present in the tangential direction only. Then, there appears an adjustable scalar parameter β, the stress jump coefficient. In case of the continuous stress, the value of the stress jump coefficient takes zero ($\beta = 0$). Similar to the effective viscosity, determination of the stress jump coefficient in the stress jump condition is also a pivotal subject. Ochoa-Tapia and Whitaker[26,27] reported that the stress jump coefficient ranges from −1 to 1.47, from the flow rate matching with the experimental results of Beavers and Joseph.[28] However, Angot[29] conducted mathematical analysis and reported that the well-posedness of the Stokes-Brinkman problem requires the stress jump coefficient being non-negative. Goyeau *et al.*[30] introduced a continuously varying heterogeneous transition layer between the homogenized fluid and porous regions and derived the stress jump coefficient in terms of the variations of the velocity and effective properties of the transition layer. Later Valdes-Parada and co-authors[31,32] theoretically analyzed the closure problems and provided an explicit expression for the stress jump coefficient as a function of the porosity independent of the characteristics of the microstructure. Tan *et al.*[33] obtained the effective viscosity and the stress jump coefficient by matching the flow rate for a channel flow over the fibrous porous media from a direct simulation with that from the analytic solutions. They reported that the effective viscosity ratio and the stress jump coefficient are from 1.2 to 14.4 and 0.3 to −2.2, respectively, for moderate and high porosities.

In authors' previous works,[19,34,35] we have attempted to explore the dual-scale flow through fibrous porous media using the Stokes-Brinkman model with the effective viscosity ($\mu_e/\mu = 1$) and stress jump coefficient ($\beta = 0.7$)[19] and characterized the anisotropic slip length at the interface between the fluid and porous media.[34,35] In the present study, by matching the slip velocity at the interface, we will present the optimal expressions of the effective viscosity and stress jump coefficient as a function of porous microstructure and fiber volume fraction using the slip length. The accuracy of the Brinkman model with such an optimal effective viscosity or optimal stress jump coefficient will be examined by comparing the velocity field from these Stokes-Brinkman simulations and from the corresponding direct simulations with the actual porous architectures. Finally, the Stokes-Brinkman coupling is employed to solve a more practical dual-scale problem of the flow around a cylindrical fiber tow. The performance of the Stokes-Brinkman coupling with the continuous stress condition and the stress jump condition will be discussed.

II. THE OPTIMAL EFFECTIVE VISCOSITY AND STRESS JUMP COEFFICIENT

A. Quantification of the effective viscosity and the stress jump coefficient

In the present work, the effective viscosity in the Stokes-Brinkman coupling and the stress jump coefficient in the Ochoa-Tapia and Whitaker model[26,27] are matched for a simple pressure-driven flow over a flat porous surface and these parameters will be used for the rest of this work. By making comparison to the analytic slip velocity of the effective Navier-slip condition at the interface, one can derive the optimal expressions of these two parameters in terms of the slip length, permeability, porosity, and porous architecture. The effective slip length for the porous surface has been already quantified accurately in authors' previous work,[34,35] and the closed form expressions for the optimal effective viscosity and the stress jump coefficient will be derived based on these expressions in this section.

We begin with a brief review of the effective Navier-slip representation for the interfacial slip over a porous medium for the completeness of this work. (Details can be found in the work of Lu and co-authors.[34,35]) Figure 1 shows a transverse flow over a fibrous porous medium with the coordinate system. The upper half of the domain ($0 < y < H$) is the fluid region Ω_f, and the lower half ($y < 0$) is the porous region Ω_p. The pressure difference is assigned in the horizontal direction. In the previous works, we reported that the effective Navier-slip condition over an imaginary smooth interface between fluid and porous media can describe the slip velocity as well as the velocity profile in the fluid domain accurately for various unidirectional porous architectures, even for anisotropic flows. The Navier-slip condition can be written as $\boldsymbol{u}_{slip} = \boldsymbol{b}\cdot(\boldsymbol{n}\cdot\nabla\boldsymbol{u})$. The symbols $\boldsymbol{b}$ and $\boldsymbol{u}_{slip}$ denote the slip length tensor and the slip velocity vector at the interface, respectively. In a simple pressure-driven channel flow over a flat surface (Fig. 1), it becomes

$$u_{slip} = b\frac{du}{dy}. \tag{5}$$

The effective slip length b has been obtained by the flow rate matching method, the original Beavers-Joseph method,[28] and it can be expressed as

$$b = \frac{(Q^* - 1)H - 6K/H}{4 - Q^*}, \tag{6}$$

where Q^* is the flow rate ratio (the ratio of the flow rate subjected to the slip boundary condition to that with the no-slip boundary condition) and H is the height of the channel. In authors' previous work,[34,35] the slip length b for various architectures and the fiber volume fractions have been calculated. For a sufficiently large channel height around ten times greater than the fiber radius, the slip length appears constant, independent of channel height, and can be considered as the property of the porous surface. Note that, due to the difference in the flow resistance in the transverse and longitudinal directions, the slip length appears anisotropic. In the present study, we only focus on the flow in the transverse direction. For a given porous interface, one can find the velocity profile as a function of the slip length, the permeability, and the height of the channel in this channel flow using the Beavers-Joseph boundary condition,[28] $du/dy = \alpha_{BJ}/\sqrt{K}(u - u_D)$, with u_D being the Darcy velocity and α_{BJ} being the dimensionless slip coefficient ($\alpha_{BJ} = \sqrt{K}/b$),

$$u(y) = \left(\frac{H/\sqrt{K}\left(H/\sqrt{K} + 2\sqrt{K}/b\right)}{2\left(1 + \sqrt{K}/b \cdot H/\sqrt{K}\right)} + \frac{\sqrt{K}/b\left(H^2/K - 2\right)}{2\left(1 + \sqrt{K}/b \cdot H/\sqrt{K}\right)} \times \left(\frac{y}{\sqrt{K}} \right) - \frac{1}{2}\left(\frac{y}{\sqrt{K}} \right)^2 \right) \cdot u_D. \quad (7)$$

In Eq. (7), the velocity at $y = 0$, the slip velocity, is now expressed in terms of the slip length

$$u_s = \frac{H/\sqrt{K} \cdot \left(H/\sqrt{K} + 2\sqrt{K}/b\right)}{2\left(1 + \sqrt{K}/b \cdot H/\sqrt{K}\right)} \cdot u_D. \quad (8)$$

In authors' early works,[34,35] we reported the slip length for various porous architecture and porosities, and interestingly, we showed that the slip length can be approximated by a single master equation independent of the porous architectures, once it is normalized and the dimensionless void length is employed. The dimensionless void length d^* is the fraction of the free surface at the interface and is defined as

$$d^* = 1 - \sqrt{\phi_s/\phi_{s\max}}, \quad (9)$$

where ϕ_s is the solid fraction (fiber area fraction) and $\phi_{s\max}$ is the maximum solid fraction in a unit cell ($\phi_{s\max} = \pi/4$ for the quadrilateral structure and $\phi_{s\max} = \pi/2\sqrt{3}$ for the hexagonal structure). Then, the dimensionless slip length, normalized by the fiber radius R, can be fitted by a single master equation

$$b^* = 0.67d^{*2.41} + 0.09, \quad b^* = b/R. \quad (10)$$

The above slip length expression can be incorporated with the Stokes-Brinkman coupling, from which the relationship between the dimensionless slip length and the effective viscosity as well as that with the stress jump coefficient can be readily obtained. We will briefly present this procedure using the analytic solution of the Stokes-Brinkman coupling in both porous and fluid domains with the given boundary conditions (Fig. 1). (See the work of Hwang and Advani[12] and Neale and Nader[16] for similar approaches.) Neglecting the inertia, flows in the fluid region can be described by the Stokes equation, and in this case, $d^2u_f/dy^2 = 1/\mu \cdot (dp/dx)$. As for the flow in the porous media, it can be described by the Brinkman equation, i.e., $\mu_e d^2u_p/dy^2 - \mu/K \cdot u_p = dp/dx$. No-slip condition is applied on the top surface. Within the porous media away from the interface, Darcy's law, i.e., $u_p = -K/\mu \cdot (dp/dx)$, needs to be recovered due to vanishing viscous stress $u_p \to u_D$, $y \to -\infty$. The problem described here is actually the same as that in obtaining the slip length in the effective Navier-slip problem (Fig. 1). At the interface, the velocity from both the regions must be continuous ($u_f = u_p$) and the stress can be either continuous (the original S-B coupling) and discontinuous (the OT-W model). The continuous stress condition can be given in this parallel flow as

$$\mu \frac{du_f}{dy} - \mu_e \frac{du_p}{dy} = 0. \quad (11)$$

The stress jump condition (Ochoa-Tapia and Whitaker[26,27]) can be written as

$$\mu_e \frac{du_p}{dy} - \mu \frac{du_f}{dy} = \mu \frac{\beta}{\sqrt{K}} u_s, \quad (12)$$

where β is the stress jump coefficient. According to Ochoa-Tapia and Whitaker,[26,27] the value of the effective viscosity is suggested as $\mu_e/\mu = 1/(1 - \phi_s)$ with the stress jump condition and therefore the stress jump coefficient β is the only adjustable parameter in their model.

Based on the governing equations and the boundary conditions above, one can obtain the solutions in the fluid region and in the porous region for the continuous stress condition and the stress jump conditions, respectively. Specifically, the slip velocity at the fluid/interface can be expressed in terms of the effective viscosity for the continuous stress condition [Eq. (13)] and in terms of the stress jump coefficient for the stress jump condition [Eq. (14)]

$$u_s = \frac{H/\sqrt{K} \cdot \left(H/\sqrt{K} + 2\sqrt{\mu_e/\mu}\right)}{2\left(1 + \sqrt{\mu_e/\mu} \cdot H/\sqrt{K}\right)} \cdot u_D \quad \text{(Continuous stress)}, \quad (13)$$

$$u_s = \frac{H/\sqrt{K} \cdot \left(H/\sqrt{K} + 2\sqrt{1/(1-\phi_s)}\right)}{2\left(1 - \beta \cdot H/\sqrt{K} + \sqrt{1/(1-\phi_s)} \cdot H/\sqrt{K}\right)} \cdot u_D \quad \text{(Stress jump)}. \quad (14)$$

By comparing the slip velocity at the interface from the work of Beavers-Joseph [Eq. (8)] with the effective slip length to the slip velocities subjected to the continuous/discontinuous stress [Eqs. (13) and (14)], one can find the closed form expressions for the relative effective viscosity (normalized by the fluid viscosity) and the stress jump coefficient as follows:

$$\frac{\mu_e{}^{\text{OPT}}}{\mu} = \frac{K}{b^2}, \quad (15)$$

$$\beta^{\text{OPT}} = \frac{\left(1/(1-\phi_s) - \sqrt{K}/b\right)\left(H^2/2K - 1\right)}{H^2/2K + H/b}. \quad (16)$$

The superscript "OPT" indicates the expressions in Eqs. (15) and (16) are optimal for both the effective viscosity and the stress jump coefficient. We have some remarks in this procedure:

(i) Matching the slip velocity using the exact slip length from the Navier-slip implies that the velocity gradient at the interface of the fluid domain is naturally described ($u_s = bdp/dn$);
(ii) The velocity gradient at the interface in the porous media domain is also predicted accurately for both cases by the interfacial stress conditions [Eqs. (11) and (12)];
(iii) The Darcy velocity away from the interface is always satisfied correctly, which is inherited from the Brinkman model with the vanishing viscous stress term;
(iv) The slip length in the present work is evaluated with the Navier-slip condition, i.e., $\boldsymbol{u}_s = b(\boldsymbol{n} \cdot \nabla \boldsymbol{u})$. On the other hand, the effective viscosity and the stress jump coefficient are estimated based on the slip velocity of Beavers-Joseph[28]

$\left(\alpha/\sqrt{K}(\boldsymbol{u}_s - \boldsymbol{u}_D) = \boldsymbol{n}\cdot\nabla\boldsymbol{u}\right)$. As mentioned in authors' previous work[34] and in the work of Saffman,[36] the error in the slip velocity is limited to $O(K)$, which is negligible in practical composites manufacturing applications.

As mentioned in the above remarks, the Stokes-Brinkman simulation with the optimal effective viscosity and stress jump coefficient can satisfy naturally for the flow in the fluid region (see "1" in Fig. 1), the slip velocity ("2") along with the stress (velocity gradient) there ("5"), and the flow within the porous media away from the interface ("4"). The remaining issue is the flow in the boundary layer ("3") with the prediction of the boundary layer thickness. In addition, a seepage flow may appear within the porous media, if the upstream flow is not exactly parallel to the fluid/porous interface, and the description of the seepage flow is another criterion for the optimal choice. We will present the performance of both the continuous stress condition and the stress jump condition in describing the flow inside the boundary layer and the seepage flow later.

Substituting the approximate expression of the slip length [Eq. (10)] into Eqs. (15) and (16) and considering the relationship between the dimensionless void length and the solid volume fraction [Eq. (9)], the optimal relative effective viscosity and the stress jump coefficient can then be expressed in closed forms as a function of the permeability, porosity, and the porous architecture,

$$\frac{\mu_e^{\mathrm{OPT}}}{\mu} = \left(\left(0.67\left(1-\sqrt{\phi_s/\phi_{s\max}}\right)\right)^{2.41} + 0.09\right)^{-2} K', \tag{17}$$

$$\beta^{\mathrm{OPT}} = \frac{\left(1/(1-\phi_s) - \sqrt{K'}\left(\left(0.67\left(1-\sqrt{\phi_s/\phi_{s\max}}\right)\right)^{2.41} + 0.09\right)^{-1}\right)\left((H/R)^2/2K' - 1\right)}{(H/R)^2/2K' + (H/R)/\left(\left(0.67\left(1-\sqrt{\phi_s/\phi_{s\max}}\right)\right)^{2.41} + 0.09\right)}. \tag{18}$$

The symbol K' denotes the normalized permeability, which can be calculated using the Gebart model,[37] i.e., $K' = \left(16/9\pi\sqrt{2}\right)\left(\sqrt{\phi_{s\max}/\phi_s} - 1\right)^{5/2}$ and $K' = \left(16/9\pi\sqrt{6}\right)\left(\sqrt{\phi_{s\max}/\phi_s} - 1\right)^{5/2}$ for the quadrilateral and the hexagonal packing structures, respectively. In Figs. 2 and 3, we present the relative effective viscosity and the stress jump coefficient as a function of the solid fraction for both quadrilateral and hexagonal structures. For comparison, those from the literature are plotted together.[13,17,23,25–27,31–33] In addition, the values of the relative effective viscosity and the stress jump coefficient along with the permeability are listed in Table I as a function of the solid fraction for the quadrilateral and the hexagonal packing structures in the transverse direction. As the solid fraction increases, the optimal relative effective viscosity decreases sharply from the factor of $O(10)$ to $O(0.01)$: $\phi_s = 0.1$, $\mu_e^{\mathrm{OPT}}/\mu = 16.909$ for quadrilateral structure, and 11.246 for hexagonal structure;

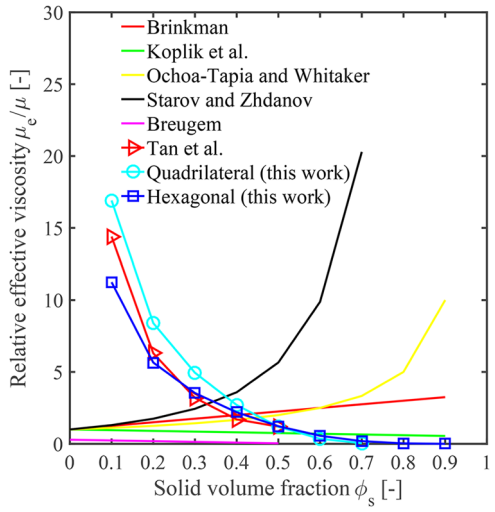

FIG. 2. The relative effective viscosity as a function of the solid volume fraction: a comparison between the present work with the literature.[13,17,23,25–27,33]

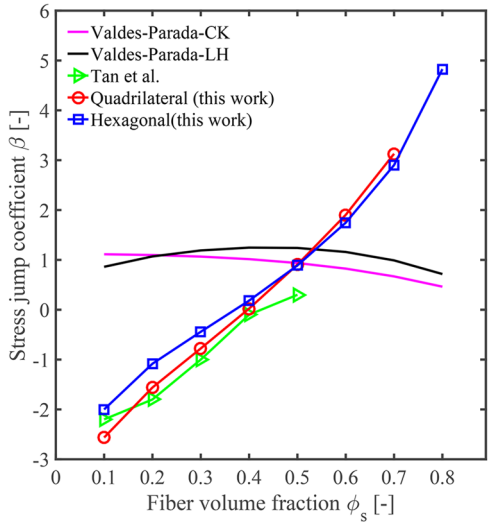

FIG. 3. The stress jump coefficient as a function of the fiber volume fraction: a comparison of the present work to results presented in the work of Valdes-Parada and co-authors.[31–33]

TABLE I. The optimal relative effective viscosity and the stress jump coefficient along with the normalized permeability as a function of the fiber volume fraction for the "Quadrilateral" and the "Hexagonal" packing structures in the transverse direction.

	Quadrilateral			Hexagonal		
ϕ_s	K/R^2	${\mu_e}^{\mathrm{OPT}}/\mu$	β^{OPT}	K/R^2	${\mu_e}^{\mathrm{OPT}}/\mu$	β^{OPT}
0.1	1.745	16.909	−2.563	1.326	11.246	−2.0
0.2	0.382	8.340	−1.561	0.313	5.655	−1.083
0.3	0.120	4.945	−0.776	0.108	3.532	−0.442
0.4	0.041	2.702	0.0227	0.042	2.196	0.183
0.5	0.013	1.190	0.906	0.016	1.227	0.888
0.6	0.003	0.353	1.904	0.006	0.563	1.747
0.7	0.0003	0.042	3.129	0.002	0.185	2.902
0.8	...	...	...	0.0002	0.030	4.827

$\phi_s = 0.7$, ${\mu_e}^{\mathrm{OPT}}/\mu = 0.042$ for quadrilateral structure, and 0.185 for hexagonal structure. With the increase in the solid fraction, the value of the stress jump coefficient increases also from negative to positive values ranging from −2.563 to 3.129 for the quadrilateral structure and −2 to 4.827 for the hexagonal structure, respectively, which is in agreement with the findings of Ochoa-Tapia and Whitaker[26,27] such that the stress jump coefficient can be either positive or negative, and it yields the value of $O(1)$. It would be worthwhile to mention the difference from the previous work of Tan *et al.*[33] Their results are limited to the fiber volume fraction from 0.1 to 0.5 with the regular packing architecture only. In the present work, we provide the effective viscosity and stress jump coefficient for a wide range of fiber volume fractions and for two different microstructures (quadrilateral and hexagonal) with explicit functional expressions.

B. Verification of the optimal effective viscosity and the stress jump coefficient

Having characterized the optimal effective viscosity and the stress jump coefficient, we validate the accuracy of the Stokes-Brinkman coupling with these two optimal parameters in describing a dual-scale flow. A flow over a flat porous medium is chosen as the test problem as shown in Fig. 4, where the flow is described in two ways: one is the flow over the actual porous architecture (quadrilateral in this case) and the other is the corresponding flow over an effective porous surface. The dimensionless channel height is set as 64 ($H/R = 64$), and the periodic boundary condition with the pressure jump is applied in the horizontal direction. Direct simulation [Fig. 4(a)] for flow over the porous media with full consideration of fibrous microstructure has been compared to the Stokes-Brinkman simulation [Fig. 4(b)] using an effective porous region characterized by the permeability K and the effective viscosity μ_e. The permeability is obtained by Gebart,[37] and the optimal effective viscosities and effective stress jump coefficients are evaluated by Eqs. (15) and (16). The direct flow simulation seeks a continuum solution based on the standard Galerkin finite-element method with the velocity and pressure as their primary unknowns. The accuracy in this direct simulation has been evaluated and validated already in authors' previous work.[34]

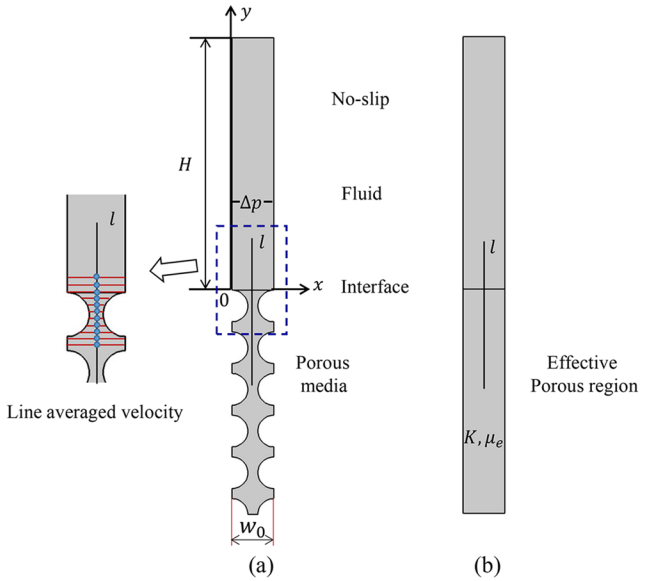

FIG. 4. The computational model for the 1D transverse flow over a fibrous porous medium. (a) A model for the direct simulation with the actual complex micro architecture; (b) the corresponding flow model for the Stoke-Brinkman coupling with a fictitious effective porous region.

To make assessment of the accuracy of the Stokes-Brinkman model, velocity fields from both the simulations need to be compared in four regions as shown in Fig. 1: (i) the velocity in the fluid region (channel flow, $0 < y < H$), (ii) the slip velocity and its slope (velocity gradient) at the interface ($y = 0$), (iii) the velocity profile in the boundary layer, and (iv) the Darcy velocity in the porous media away from the interface.

In direct simulations, the entire flow region [Fig. 4(a)] is solved with the Stokes equation [Eq. (1)] and a unit pressure drop is applied in the flow direction, considering additional no-slip boundary condition on the fiber boundaries and the bottom and top walls. To implement the Stokes-Brinkman coupling [Fig. 4(b)], we separately solve the Stokes equation for the flow in the fluid region ($0 < y < H$) and the Brinkman equation for the flow in the porous media ($y < 0$). At the fluid/porous interface ($y = 0$), the velocity is considered to be continuous ($\boldsymbol{u}_f = \boldsymbol{u}_p$), with which the stress balance is naturally satisfied for the continuous stress condition. In case of the stress jump condition, according to Eq. (12), an additional weak contribution in the weak form of the momentum equation is assigned at the interface for the jump stress $\int_{\partial\Omega_f \cap \partial\Omega_p} \mu\beta/\sqrt{K}(\boldsymbol{u}\cdot\boldsymbol{v})d\Gamma$, with $\boldsymbol{v}$ being a test function. COMSOL Multiphysics 4.4 is employed to implement all the simulations with the quadrilateral velocity and linear pressure interpolations. Although not presented here, mesh convergence has been checked until the relative error in slip coefficient appears $O(10^{-3})$, as was done in the work of Lu *et al.*[34] Plotted in Fig. 5 are the velocity profiles along the line "l" (see Fig. 4) passing through the centerline of the periodic unit domain, from direct simulations and that from the Stokes-Brinkman coupling using either the continuous stress condition or the stress jump condition for various fiber volume fractions: $\phi_s = 0.1$ [Fig. 5(a)],

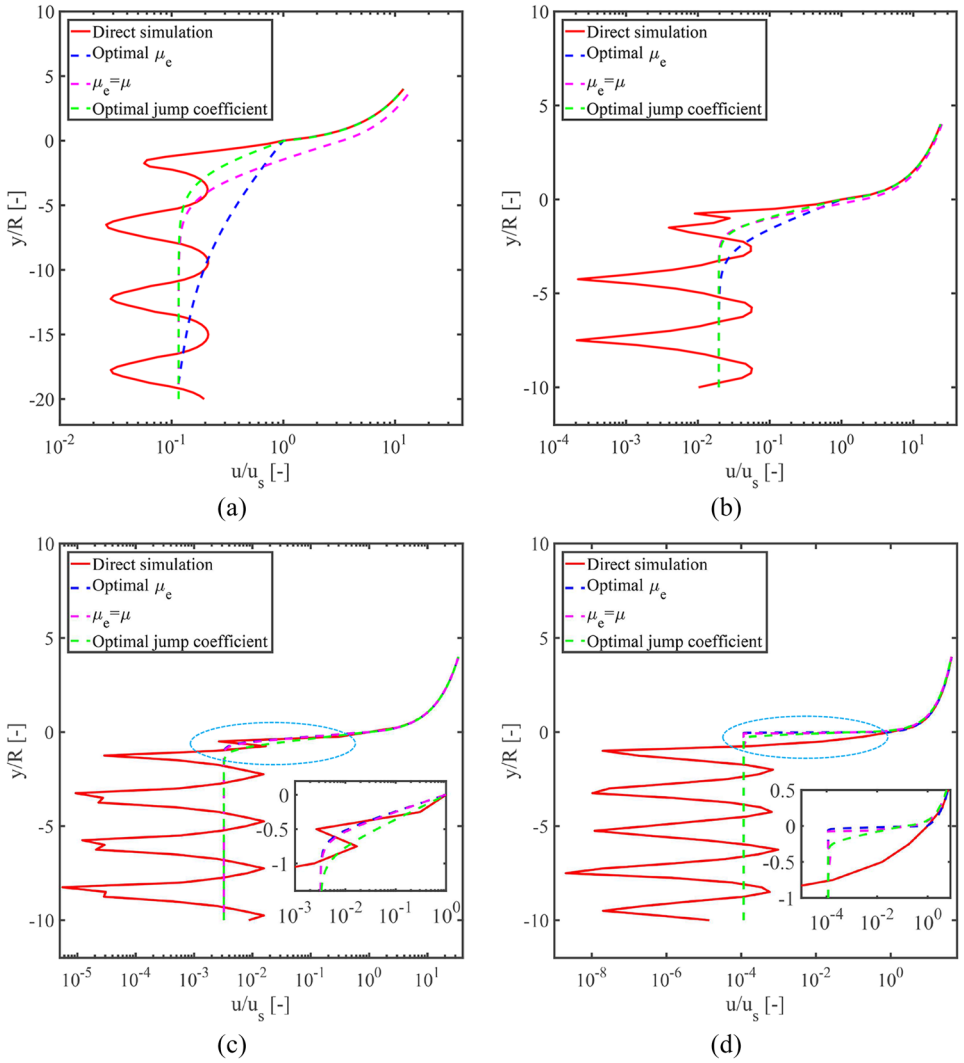

FIG. 5. Velocity profiles along the line "*l*" (indicated in Fig. 4) from the direct simulations and the Stokes-Brinkman coupling with the optimal effective viscosity ratios and the optimal stress jump coefficients for the quadrilateral structure. Results from the identical effective viscosity ratios are also plotted for comparison: (a) $\phi_s = 0.1$, $\mu_e^{OPT}/\mu = 16.91$, $\beta^{OPT} = -2.563$; (b) $\phi_s = 0.3$, $\mu_e^{OPT}/\mu = 4.95$, $\beta^{OPT} = -0.776$; (c) $\phi_s = 0.5$, $\mu_e^{OPT}/\mu = 1.19$, $\beta^{OPT} = 0.906$; and (d) $\phi_s = 0.7$, $\mu_e^{OPT}/\mu = 0.04$, $\beta^{OPT} = 3.129$.

$\phi_s = 0.3$ [Fig. 5(b)], $\phi_s = 0.5$ [Fig. 5(c)], and $\phi_s = 0.7$ [Fig. 5(d)]. In each case, we present the velocity profiles from direct simulation and the Stokes-Brinkman coupling with the optimal effective viscosity and that with the optimal stress jump coefficient. The results from the Stokes-Brinkman coupling with the identical effective viscosity ($\mu_e = \mu$), a common choice in the literature,[19–21] are also presented for comparison. Note that the line "*l*" starts from the fluid region, passing through the fluid/porous interface and ends in the Darcy region within the porous media. Due to the complex flow behavior near the interface, we applied the line averaged velocity as shown in Fig. 4 to obtain the macroscale properties, i.e., $u(y) = 1/w_0 \int u dx$, with w_0 being the width of the unit flow region. From the results in Fig. 5, one can observe that solutions from both the continuous stress condition with the optimal effective viscosities and the stress jump condition with the optimal stress jump coefficients agree well with that from the direct simulations for various fiber volume fractions, for both the flow in the fluid region ("1" in Fig. 1) and in the porous region ("4"). Moreover, both these two optimal solutions can accurately predict the slip velocities as well as the slopes at the interface ("2"). However, a significant discrepancy is observed with the identical relative effective viscosity ($\mu_e = \mu$), particularly for low solid volume fractions. For example, in case of the solid volume fraction of 0.1, the slip velocity from the identical effective viscosity is found around 3 times larger than that from the direct simulation. As for the velocity profile in the boundary layer, although it is not easy to clearly identify the boundary layer from the direct simulations, one can summarize the observations as follows: (i) for low fiber fractions ($\phi_s = 0.1$ and $\phi_s = 0.3$), the optimal continuous stress condition seems to overpredict the boundary layer, whereas the optimal jump stress condition predicts its thickness better; (ii) for medium ($\phi_s = 0.5$) and high ($\phi_s = 0.7$) fiber fractions, the optimal continuous stress condition underestimate the boundary layer thickness, compared to the optimal stress jump condition. The accuracy in the prediction of the boundary layer thickness of the

TABLE II. The relative error of slip velocity and the relative error norm of velocity distribution in the fluid region in the flat channel flow for different fiber volume fractions with various stress boundary conditions.

	Continuous stress condition				Stress jump condition with optimal β	
	$\mu_e = \mu$		Optimal μ_e			
ϕ_s	E_{slip} (%)	E_{vel} (%)	E_{slip} (%)	E_{vel} (%)	E_{slip} (%)	E_{vel} (%)
0.1	237.35	324.23	0.84	1.15	3.02	4.13
0.3	97.7	112.37	0.45	0.52	0.72	0.83
0.5	4.51	4.92	0.66	0.72	0.59	0.64
0.7	79.6	84.5	4.98	5.29	4.12	4.37

continuous stress condition with the optimal effective viscosity is found to depend strongly on the fiber volume fraction. However, this drawback of the Stokes-Brinkman coupling with effective viscosity seems not to be serious concern in a practical situation with medium and high fiber volume fraction on composite manufacturing. In addition, the relative error of slip velocity and the relative error norm of velocity distribution in the fluid region for different fiber volume fractions with various stress boundary conditions are listed in Table II.

III. FLOW OVER A CYLINDRICAL FIBER TOW

The Stokes-Brinkman coupling with both the continuous stress condition and the stress jump condition has been applied and validated in describing the coupled flow with flat interfaces. A challenging issue remains how to deal with the Stokes-Brinkman coupling, when the shape of interface is curved, for example, the cross sections of the reinforcements or the fiber tows are usually elliptic in the liquid composite manufacturing. In this section, we will solve an example problem for a flow over a fibrous porous medium in which the shape of the interface is curved. As shown in Fig. 6(a), there is a

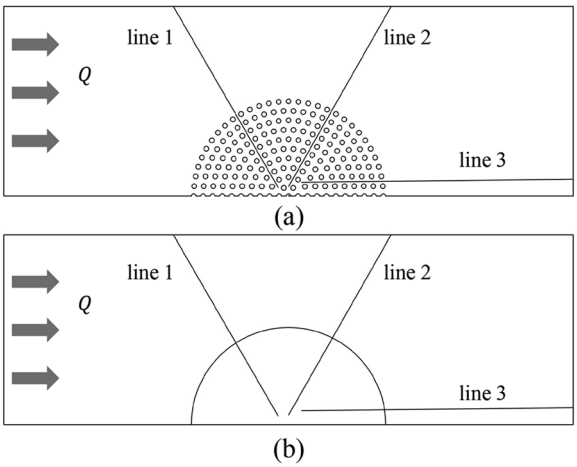

FIG. 6. A schematic description of an example flow over a cylindrical dual-scale porous tow: (a) the direct simulation for flow through arrays of cylinders and (b) the Stokes-Brinkman coupling with a fictitious cylindrical porous region.

flow over/through arrays of cylinders, which are arranged similar to the hexagonal pattern. Figure 6(b) is a flow over/through an effective porous region characterized by the permeability K and the effective viscosity μ_e.

Before investigating the applicability of the Stokes-Brinkman coupling in describing such a complex coupled flow, the permeability should be first characterized accurately. As the permeability is involved in evaluating both the Stokes-Brinkman equation and the effective viscosity/stress jump coefficient through the slip length, the evaluation and application of the correct permeability is of great importance. We remark that the permeability in the slip length expression [Eq. (6)] (a "local" permeability) might be different from the permeability in the Stokes-Brinkman equation [Eq. (2)] (a "global" permeability). Note that the slip length depends solely on the local quantity at the interface, which implies that it can be estimated by the local fiber structures (hexagonal in this case), particularly by the structure on the outer-most layer.[34] Therefore, the Gebart expression[37] for the permeability and Eq. (6) have been employed to estimate the local slip length and therefore the effective viscosity and the stress jump coefficient. According to Table I, the values of the optimal relative effective viscosity μ_e^{OPT}/μ and the stress jump coefficient β^{OPT} are 5.655 and −1.083, respectively, for the hexagonal structure ($\phi_s = 0.2$). Note that the stress jump condition in this problem is applied only in the tangential direction as shown in Eq. (4) and the tangent vector along the surface, where the stress jump is applied, varies with the cylindrical tow interface.

On the other hand, one needs a "global" permeability as well to perform the flow simulation with the Stokes-Brinkman equation. Unlike the local permeability for the slip length, the global permeability is the Darcy permeability that relates the pressure drop and the flow rate. The global permeability of the cylindrical fiber tow is often estimated using the radial flow (see the work of Sozer and Advani[38]) as follows:

$$K = Q_r \frac{\mu}{2\pi} \frac{\ln(r_0/r_m)}{p_i - p_0}. \tag{19}$$

The symbols Q_r, r_m, r_0, p_i, and p_0 are the radial flow rate, the radial position for pressure measurement, the outer radius of the cylindrical porous region (in this case is 10.252 mm), the measured pressure at the radial position r_m, and the pressure at the interface at r_0, which is usually the atmospheric pressure. The fiber volume fraction of the tow is measured as 0.2, considering cylindrical porous

media of radius r_0. COMSOL Multiphysics 4.4 is employed to implement the simulations in this example flow problem. Although not presented here, we have tested the mesh refinement characteristics to ensure the accuracy more than three digits in estimating the global permeability. Various pressure measurement positions r_m have been employed to estimate the permeability, and the difference in the global permeability on the choice of r_m is found to be negligibly minor. Consequently, we adopt the pressure measurement position r_m being $r_m/r_0 = 0.434$ and the corresponding permeability is found to be 2.22×10^{-8} m^2, which is 10% larger than the local permeability of a hexagonal fiber packing for the same fiber fraction ($\phi_s = 0.2$).[37]

To understand the performance of the Stokes-Brinkman coupling in describing the coupled flow with a curved interface, we would like to exam the velocity profiles along three lines from the direct simulation [Fig. 6(a)] and from the Stokes-Brinkman coupling [Fig. 6(b)], where both the continuous stress condition and the stress jump condition with the optimal parameters have been applied. For the continuous stress condition, a velocity profile from the identical effective viscosity ($\mu_e = \mu$) is plotted as well for comparison. The results are presented in Fig. 7. In general, along line 1 and line 2 [Figs. 7(a) and 7(b)], once the optimal parameters are applied, the Stokes-Brinkman coupling with both the continuous/jump stress conditions can match the velocity profiles in the entire domain accurately. The continuous stress condition with the conventional identical effective viscosity fails to predict the slip velocity at the interface (with the error being 174% for line 1 and 178% for line 2). The estimation of the slip velocity has been improved significantly, once the optimal parameters are chosen. For example, the error of the slip velocity from the continuous stress condition with the optimal effective viscosity is found around 29.5% for line 1 and 29.8% for line 2. Similarly, the error of the slip velocity from the stress jump condition with the optimal stress jump coefficient is around 21.6% for line 1 and 22.1% for line 2. As for line 3, all these three conditions yield a relatively good prediction in estimating the slip velocity, with the error being 12.6% for the continuous stress condition with the conventional identical effective viscosity, 13.2% for the continuous stress condition with the optimal effective viscosity and

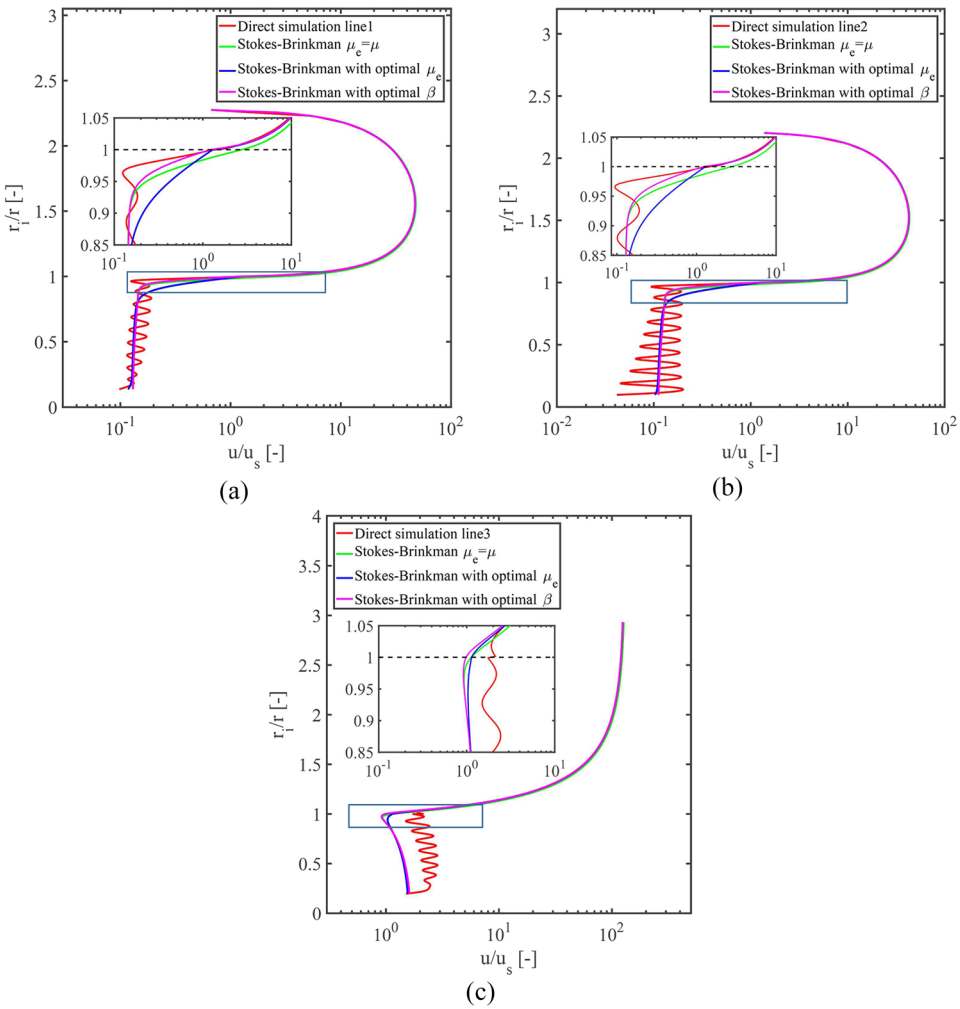

FIG. 7. Velocity profiles along three lines (indicated in Fig. 6) from the direct simulation and the Stokes-Brinkman coupling with the continuous stress condition and the stress jump condition: (a) along the line 1, (b) along the line 2, and (c) along the line 3.

TABLE III. The relative error of slip velocity and the relative error norm of velocity distribution in the fluid region along three lines in the flow over a cylindrical fiber tow (Fig. 6) with various stress boundary conditions.

	Continuous stress condition				Stress jump condition with optimal β	
	$\mu_e = \mu$		Optimal μ_e			
	E_{slip} (%)	E_{vel} (%)	E_{slip} (%)	E_{vel} (%)	E_{slip} (%)	E_{vel} (%)
Line 1	174	182.39	29.5	31.43	21.6	23.18
Line 2	178	192.07	29.8	30.80	22.1	22.99
Line 3	12.6	29.12	13.2	13.55	1.8	2.09

1.8% for the stress jump condition with the optimal stress jump coefficient. The relative error of slip velocity and the relative error norm of velocity distribution in the fluid region along these three lines with various stress boundary conditions are listed in Table III.

In addition, similar to the results in Sec. II B, the continuous stress condition with the optimal effective viscosity again overestimates the boundary layer thickness, while the stress jump condition with the optimal stress jump coefficient yields much improved behaviors. Along the line 3, which is perpendicular to the porous interface, one can observe the performance for the prediction of the seepage flow and, as shown in Fig. 7(c), both the optimal parameters fail to yield correct "Darcy" velocity. In fact, there appears a "shift" around 50% of the velocity from the direct simulation. This may arise from the fact that both the optimal effective viscosity and the stress jump coefficient are derived from the Navier-slip length b, whereas the Navier-slip condition requires the flow direction parallel to the interface. Therefore, the Stokes-Brinkman coupling itself with both the optimal parameters has a deficiency in describing such an impinging seepage flow.

IV. CONCLUSIONS

The optimal effective viscosity and the stress jump coefficient in the Stokes-Brinkman coupling for flows in dual-scale porous media have been accurately characterized, using the slip length, which can be obtained from the Navier-slip boundary condition. The correlations between the slip length and the effective viscosity as well as the stress jump coefficient are rigorously derived in this work. Once the optimal parameters are chosen (i.e., the effective viscosity and the stress jump coefficient), both the continuous stress condition and the stress jump condition in the Stokes-Brinkman coupling can describe the flow field in a channel with a porous surface, reproducing accurate velocity profile inside the fluid channel, the slip velocity as well as its gradient (stress) at the fluid/porous interface and Darcy's velocity within the porous wall. For the flow in a thin boundary layer beneath the interface, the continuous stress condition fails to predict the boundary layer thickness particularly for very small volume fractions, whereas the stress jump condition can reproduce them well, even for very low volume fraction. In addition, both of these optimal parameters fail to yield the correct impinging seepage flow. Improvement of the Stokes-Brinkman model for the seepage flow is the subject of the future investigation.

It is worthwhile to mention that, in our approach, both the effective viscosity and the stress jump coefficient might be considered as a property of the porous media. As reported in authors' previous work,[34] once the channel height is large enough compared to the fiber radius, for example, $H/R > 10$, the Navier-slip length b solely depends on the outmost microstructure of the interface: the dimensionless void length d^*, which in fact is the fraction of the free slip region at the porous interface. For a given porous structure, the optimal values of the effective viscosity and the stress jump coefficient are easily determined since both of these two parameters are derived from the slip length b [see Eqs. (15) and (16)]. By accurately characterizing the optimal effective viscosity or the stress jump coefficient, the Brinkman model with a macroscopically characterized porous domain can be applied to replace the microstructural fibrous porous media, with which the computational cost will be reduced considerably when dealing with void formation/transport and particle deposition/filtration.[10–12] The optimal values of the effective viscosity and of the stress jump coefficient obtained in this work (see Table I) may provide an effective framework in describing a flow in dual-scale porous media.

ACKNOWLEDGMENTS

The authors acknowledge financial support from the National Research Foundation of Korea (Grant No. NRF-2019R1A2C1003974) and from the Ministry of Trade, Industry and Energy, Korea (the Industrial Strategic Technology Development Program, Grant No. 10062514).

REFERENCES

[1] J. Bear and A. Verruijt, *Modeling Groundwater Flow and Pollution* (Springer Science & Business Media, 2012), Vol. 2.
[2] N. Chen, M. Gunzburger, and X. Wang, "Asymptotic analysis of the differences between the Stokes–Darcy system with different interface conditions and the Stokes–Brinkman system," J. Math. Anal. Appl. **368**, 658 (2010).
[3] P. Daripa and C. Gin, "Studies on dispersive stabilization of porous media flows," Phys. Fluids **28**, 082105 (2016).
[4] J. M. van der Meer, R. Farajzadeh, W. R. Rossen, and J. D. Jansen, "Influence of foam on the stability characteristics of immiscible flow in porous media," Phys. Fluids **30**, 014106 (2018).
[5] B. Ling, M. Oostrom, A. M. Tartakovsky, and I. Battiato, "Hydrodynamic dispersion in thin channels with micro-structured porous walls," Phys. Fluids **30**, 076601 (2018).

[6]D. Maggiolo, F. Picano, and M. Guarnieri, "Flow and dispersion in anisotropic porous media: A lattice-Boltzmann study," Phys. Fluids **28**, 102001 (2016).
[7]M. A. Spaid and F. R. Phelan, Jr., "Lattice Boltzmann methods for modeling microscale flow in fibrous porous media," Phys. Fluids **9**, 2468 (1997).
[8]M. Griebel and M. Klitz, "Homogenization and numerical simulation of flow in geometries with textile microstructures," Multiscale Model. Simul. **8**, 1439 (2010).
[9]D. Niedziela, J. Troltzsch, A. Latz, and L. Kroll, "On the numerical simulation of injection molding processes with integrated textile fiber reinforcements," J. Thermoplast. Compos. Mater. **26**, 74 (2013).
[10]J. J. Gangloff, Jr., W. R. Hwang, and S. G. Advani, "Characterization of bubble mobility in channel flow with fibrous porous media walls," Int. J. Multiphase Flow **60**, 76 (2014).
[11]J. J. Gangloff, Jr., W. R. Hwang, and S. G. Advani, "The investigation of bubble mobility in channel flow with wavy porous media walls," Int. J. Multiphase Flow **70**, 1 (2015).
[12]W. R. Hwang, S. G. Advani, and S. Walsh, "Direct simulations of particle deposition and filtration in dual-scale porous media," Composites, Part A **42**, 1344 (2011).
[13]H. C. Brinkman, "A calculation of the viscous force exerted by a flowing fluid on a dense swarm of particles," Flow, Turbul. Combust. **1**, 27 (1949).
[14]J. C. Slattery, "Single-phase flow through porous media," AIChE J. **15**, 866 (1969).
[15]G. Ooms, P. F. Mijnlieff, and H. L. Beckers, "Frictional force exerted by a flowing fluid on a permeable particle, with particular reference to polymer coils," J. Chem. Phys. **53**, 4123 (1970).
[16]G. Neale and W. Nader, "Practical significance of Brinkman's extension of Darcy's law: Coupled parallel flows within a channel and a bounding porous medium," Can. J. Chem. Eng. **52**, 475 (1974).
[17]W. Breugem, "The effective viscosity of a channel-type porous medium," Phys. Fluids **19**, 103104 (2007).
[18]T. S. Lundgren, "Slow flow through stationary random beds and suspensions of spheres," J. Fluid Mech. **51**, 273 (1972).
[19]W. R. Hwang and S. G. Advani, "Numerical simulations of Stokes–Brinkman equations for permeability prediction of dual scale fibrous porous media," Phys. Fluids **22**, 113101 (2010).
[20]A. Tamayol, A. Khosla, B. L. Gray, and M. Bahrami, "Creeping flow through ordered arrays of micro-cylinders embedded in a rectangular minichannel," Int. J. Heat Mass Transfer **55**, 3900 (2012).
[21]A. Tamayol, J. Yeom, M. Akbari, and M. Bahrami, "Low Reynolds number flows across ordered arrays of micro-cylinders embedded in a rectangular micro/minichannel," Int. J. Heat Mass Transfer **58**, 420 (2013).
[22]J. A. Kołodziej, M. Mierzwiczak, and J. K. Grabski, "Computer simulation of the effective viscosity in Brinkman filtration equation using the Trefftz method," J. Mech. Mater. Struct. **12**, 93 (2017).
[23]J. Koplik, H. Levine, and A. Zee, "Viscosity renormalization in the Brinkman equation," Phys. Fluids **26**, 2864 (1983).
[24]S. Kim and W. B. Russel, "Modelling of porous media by renormalization of the Stokes equations," J. Fluid Mech. **154**, 269 (1985).
[25]V. M. Starov and V. G. Zhdanov, "Effective viscosity and permeability of porous media," Colloids Surf., A **192**, 363 (2001).
[26]J. A. Ochoa-Tapia and S. Whitaker, "Momentum transfer at the boundary between a porous medium and a homogeneous fluid—I. Theoretical development," Int. J. Heat Mass Transfer **38**, 2635 (1995).
[27]J. A. Ochoa-Tapia and S. Whitaker, "Momentum transfer at the boundary between a porous medium and a homogeneous fluid—II. Comparison with experiment," Int. J. Heat Mass Transfer **38**, 2647 (1995).
[28]G. S. Beavers and D. D. Joseph, "Boundary conditions at a naturally permeable wall," J. Fluid Mech. **30**, 197 (1967).
[29]P. Angot, "On the well-posed coupling between free fluid and porous viscous flows," Appl. Math. Lett. **24**, 803 (2011).
[30]B. Goyeau, D. Lhuillier, D. Gobin, and M. G. Velarde, "Momentum transport at a fluid–porous interface," Int. J. Heat Mass Transfer **46**, 4071 (2003).
[31]F. J. Valdes-Parada, B. Goyeau, and J. A. Ochoa-Tapia, "Momentum stress jump condition at the fluid-porous boundary: Prediction of the jump coefficient," in Proceedings of the AIChE National Meeting, San Francisco, USA, 2006.
[32]F. J. Valdés-Parada, B. Goyeau, and J. A. Ochoa-Tapia, "Jump momentum boundary condition at a fluid–porous dividing surface: Derivation of the closure problem," Chem. Eng. Sci. **62**, 4025 (2007).
[33]H. Tan, X. Chen, K. M. Pillai, and T. D. Papathanasiou, "Evaluation of boundary conditions at the clear-fluid and porous-medium interface using the boundary element method," in Flow Processes in Composite Materials-9 (FPCM-9), Montreal, Canada, 2008.
[34]J. Lu, H. K. Jang, S. B. Lee, and W. R. Hwang, "Characterization on the anisotropic slip for flows over unidirectional fibrous porous media for advanced composites manufacturing," Composites, Part A **100**, 9 (2017).
[35]J. Lu, H. K. Jang, and W. R. Hwang, "Data on the anisotropic interfacial slip length over fibrous porous media," Data Brief **13**, 453 (2017).
[36]P. G. Saffman, "On the boundary condition at the surface of a porous medium," Stud. Appl. Math. **50**, 93 (1971).
[37]B. R. Gebart, "Permeability of unidirectional reinforcements for RTM," J. Compos. Mater. **26**, 1100 (1992).
[38]E. M. Sozer and S. G. Advani, *Process Modeling in Composites Manufacturing* (CRC Press, 2010).